

UNCLASSIFIED

Defense Technical Information Center Compilation Part Notice

ADP010516

TITLE: Alenia Multidisciplinary Design
Optimization - Topics and Approaches

DISTRIBUTION: Approved for public release, distribution unlimited

This paper is part of the following report:

TITLE: Aerodynamic Design and Optimisation of
Flight Vehicles in a Concurrent
Multi-Disciplinary Environment [la Conception et
l'optimisation aerodynamiques des vehicules
aeriens dans un environnement pluridisciplinaire
et simultane]

To order the complete compilation report, use: ADA388284

The component part is provided here to allow users access to individually authored sections of proceedings, annals, symposia, ect. However, the component should be considered within the context of the overall compilation report and not as a stand-alone technical report.

The following component part numbers comprise the compilation report:

ADP010499 thru ADP010530

UNCLASSIFIED

Alenia Multidisciplinary Design Optimisation - Topics and Approaches

V. Selmin*, P.L. Vitagliano, A. Pennavaria and L. Crosetta

*Alenia Aerospazio - Divisione Aeronautica
SPRT, Corso Marche 41
10146 Torino, Italy

Abstract

The purpose of this paper is to report on methods which have been developed or which are under development at Alenia Aeronautica for multidisciplinary optimum design, with particular emphasis on aerodynamic shape design. Results of transonic 2D and 3D optimisation problems are presented.

1 INTRODUCTION

Multidisciplinary Design Optimisation (MDO) will provide designers a new array tools and approaches that will take them closer to that elusive goal, an "optimum airplane". MDO has been defined as "a formal design methodology based on integration of disciplinary analysis and sensitivity analysis, optimisation and artificial intelligence, applicable at all stages of the multidisciplinary design of aerospace systems". What this really means is that MDO is a way of getting engineers from various disciplines, such as aerodynamics, structures, weights, control systems, propulsion, etc., to work together. Mathematical tools, such as sensitivity analysis, modelling methods, and optimisation solvers, provide a mechanism by which this working together can be accomplished. The result is a process that can both reduce the design cost and flow-time, and improve the quality of aerospace systems.

Since the early nineties, Alenia Aeronautica has improved its optimisation design capability by participating to several ECC funded initiatives on optimisation (EUROPT, ECARP, MDO). The result is a highly automatised system that allows to solve near real life design problems. This paper describes in some details the optimisation system and its potentialities. In particular, the multidisciplinary (aerodynamics+structure) optimisation design of a wing-body configuration is presented. Although the system we have developed is general, emphasis will be done in the following to wing like geometries which are the subject of the section dedicated to applications.

2 OPTIMISATION SYSTEM

From a mathematical point of view, in order to solve an optimisation problem, the values assigned to the design variables \mathbf{X} must be found so as to minimize the objective function $F(\mathbf{X})$ while maintaining that the possible constraint functions $G_j(\mathbf{X})$ are ≤ 0 . The designer must derive these functions and choose the design variables that govern the transformation of the geometry.

The optimisation framework which was developed is formed by an optimisation module, an analysis module and an interface module that handles the geometry modifications (Fig. 1). The interface module is integrated within a Multi-Model Generator which provides the CFD system with a discretisation of the wing geometry and the CSM system with a finite element model of the wing torsion box and the forces acting on the model reference axis.

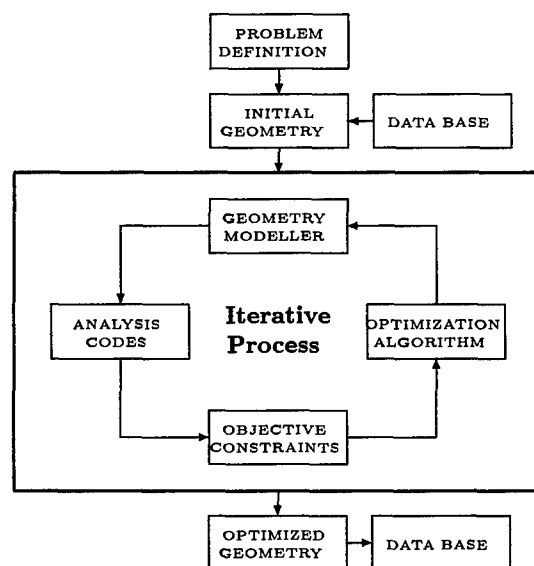


Figure 1: Optimisation system.

The optimisation module is based on optimisation routines coming from the commercial package ADS[1]. For unconstrained problems, a quasi-Newton method like the BGFS variable metric method is usually used; while for constrained problems, a method based on Zoutendijk's feasible direction algorithm[2] was selected. The optimisation routines are coupled with analysis codes which give the value of the derivatives of the objective function and of the constraints. Based on these derivatives, the optimisation routine chooses the most suitable modification direction. Aerodynamic coefficients are computed by using in-house CFD solvers, while wing mass is estimated through MSC NASTRAN structural optimisation module. The design variables can be any of the wing planform defining parameters or those that govern the modification of selected wing section shapes. The parametrisation technique is based on a shape perturbation method.

3 PARAMETRISATION

The wing is defined by:

- 1- The planform defining parameters such area(S), aspect ratio(AR) and sweep angle($Sweep$).
- 2- The twist (Tw) and thickness (Tc) of key wing sections.
- 3- The shape of the key wing sections, which is generally given by the coordinates of a set of nodes.

Each section is defined with respect to a local frame, centred at the section leading edge and having the x -axis coincident with the section chord. Normalised coordinates are introduced by scaling each length with the chord length, which means that $x \in [0, 1]$.

In the parametric model, the shape is modified using the following representation:

$$\begin{aligned} x(t) &= x^*(t) \equiv t & t \in [0, 1] \\ z(t) &= z^*(t) + \sum_{j=1}^n \Delta z_j B_{j,n}(t) \end{aligned}$$

where (x^*, z^*) represents the position vector of the original shape and $B_{j,n}$ are general shape modification functions. The design variables are the parameters Δz_j . The original shape is recovered if they are all zero.

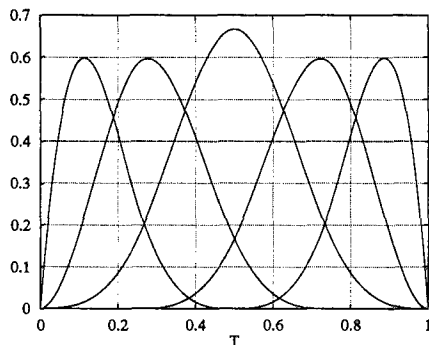


Figure 2: B-spline functions.

The present method greatly reduces the number of design variables with respect to a spline defining curve approach and may lead to a strong reduction on the computational cost of the optimisation. Various shape functions, including Hick-Henne functions[3], Bernstein polynomials and B-spline functions[4], have been studied. Among those, B-spline approach is preferred whereas the functions have a more compact support and allow to modify only locally the shape. Fig. 2 illustrates the 7th-order uniform cubic B-spline functions, which represents the default option implemented into the optimisation system. Only ten design variables are required to modify both upper and lower active wing section surfaces. Those sections without a design variables specified value are modified from the design variables associated to neighbouring sections using a linear relationship.

4 ANALYSIS TOOLS

4.1 Aerodynamic analysis

The aerodynamic analysis is performed using simulation systems based on in-house developed Euler and Navier-

Stokes multiblock structured or unstructured solvers. Both take advantage of explicit time marching schemes employing finite-volume-based central difference spatial discretisations. Multiblock solvers are cell-centred based, while unstructured ones use a node-centred/cell-vertex approach. Nonlinear second-order and linear fourth-order damping terms are added for stability and shock-capturing properties. Time integration is performed using multistage algorithm. Convergence to steady state is accelerated with the aid of local time stepping, implicit residual smoothing and enthalpy damping (inviscid computations only). For turbulence modelling, Baldwin-Barth one-equation, together with $k-\omega$ and $k-R_t$ two-equation models are available. The unstructured solvers can accepted structured multiblock grids as input, which are converted into unstructured one-block meshes.

The flow solvers are implemented, together with a mesh generator and a procedure for domain modelling. Those allow automatic remeshing of the new geometry and of the associated field grid, during the optimisation, as the design parameters are modified. As an alternative, a Laplacian smoothing based node movement algorithm was developed. It has the capability to deform a grid while maintaining the characteristics of the initial one. This allows to introduce an automatic mesh deformation tool within the optimisation process, which we consider of paramount importance in order to deal with very complex geometries and with unstructured grids.

4.2 Mesh deformation algorithm

In the following, \mathbf{x}_i will indicate the position vector of node i . We will indicate with \mathcal{E}_i the set of elements belonging to the patch \mathcal{P}_i of elements surrounding a given internal node i . \mathcal{K}_i is instead the set formed by the nodes on the boundary of \mathcal{P}_i .

The method is based on an edge based data structure which has originally been developed for unstructured finite volume CFD codes. To move the mesh, it is first assumed that each node i of the grid is connected to each adjacent node j by a fictitious spring under the force \mathbf{F}_{ij} defined by

$$\mathbf{F}_{ij} = K_{ij} (\mathbf{x}_j - \mathbf{x}_i) = K_{ij} \Delta \mathbf{x}_{ij} \quad (1)$$

where K_{ij} is the spring constant which, in general, will depend on some local grid features (grid metrics).

The resulting mesh is the solution of the equilibrium system for each vertex i :

$$\sum_{j \in \mathcal{K}_i} \mathbf{F}_{ij} = 0, \quad (2)$$

which is also equivalent to minimize the energy of the overall spring system

$$\frac{1}{2} \sum_{j \in \mathcal{K}_i} K_{ij} \Delta \mathbf{x}_{ij}^2. \quad (3)$$

In order to modify the grid while maintaining it close to the initial mesh characteristics, additional terms are introduced which modify the spring energy relation as follows

$$\frac{1}{2} \sum_{j \in \mathcal{K}_i} K_{ij} (\Delta \mathbf{x}_{ij} - \mathbf{Q}_{ij} \Delta \mathbf{x}_{ij}^0)^2 \quad (4)$$

where \mathbf{x}_i^0 is the vector position of node i in the initial grid and \mathbf{Q} is a mesh adaptation transformation matrix, which is related to the change between the original and deformed surface shapes. In the case of

$$\mathbf{Q} = \mathbf{I} \quad \text{and} \quad \Delta \mathbf{x}_{ij} = \Delta \mathbf{x}_{ij}^0,$$

the spring energy is zero and the grid nodes do not move.

A conjugate gradient method is used to minimize the modified spring energy equation 4. The technique is valid for both regular and irregular grids.

Fig. 3 illustrates the application of the node movement method to the grid deformation which results from a 50% thickness increase of the NACA0012 airfoil.

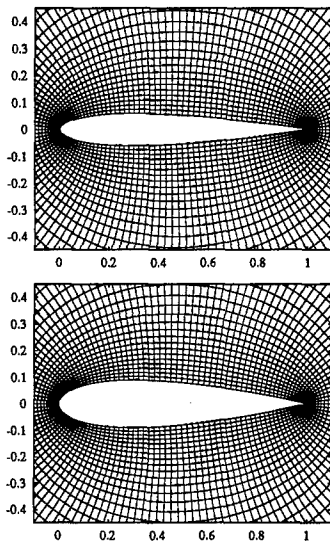


Figure 3: Mesh deformation: 50% increase in thickness.

4.3 Structural analysis

Starting from the finite element and loads models provided by the Multi-Model Generator, the wing mass is computed using the structural optimisation module of the MSC/NASTRAN code. The Sequential Quadratic Programming minimisation method is usually selected.

5 OPTIMISATION ALGORITHM

At each iteration q of the minimization process, the design vector \mathbf{X} is updated according to the formula $\mathbf{X}^q = \mathbf{X}^{q-1} + \omega \mathbf{S}^q$, where \mathbf{S}^q is a unit vector representing a search direction in a space having as many dimensions as the design variables, and where ω defines the displacement in the direction \mathbf{S}^q . In the Method of Feasible Direction, the search direction is built in such a way that it will reduce the objective function without violating the constraint for some finite move, and thus can be defined as a constrained steepest descent direction. The search direction \mathbf{S} is determined by considering the following problem:

Minimize:

$$\nabla F(\mathbf{X}) \cdot \mathbf{S}$$

Subject to:

$$\begin{aligned} \nabla G_j(\mathbf{X}) \cdot \mathbf{S} &\leq 0 \\ \mathbf{S} \cdot \mathbf{S} &\leq 1 \end{aligned}$$

The last inequality is introduced to ensure that the search vector remains bounded. Solving this problem gives a search direction which is tangent to the critical constraint boundaries, unless the objective can be reduced more rapidly by moving away from one or more constraints.

In the optimization process, the gradients are calculated by a first order forward finite difference unless a variable is at its upper bound. In this case, a first order backward finite difference step is used.

6 APPLICATIONS

6.1 Single-point airfoil optimisation

The TE3 test case [5] addresses the problem of drag minimisation in transonic flows. Far field conditions are $M_\infty = 0.73$ and an angle of attack $\alpha = 2^\circ$. The RAE2822 airfoil has been used as the starting profile. The objective was to search for a minimum drag based on a given lift coefficient. Although this test case was defined as an inviscid one, optimisation on the basis of a viscous flow has been additionally performed. Two different test cases were run:

1. An inviscid optimisation based on the above flow parameters and the constraint that the lift coefficient for $\alpha = 2^\circ$ ($c_l = 0.865$) had to be kept unchanged.
2. A viscous optimisation with the same flow conditions as above, a lift coefficient of $c_l = 0.648$, a Reynolds number $Re = 6.5 \cdot 10^6$ and a transition fixed at $x/c = 0.03$.

Additional constraints have been applied to both test cases. These constraints read: $t/c = (t/c)_{\text{RAE2822}}$, α is kept fixed.

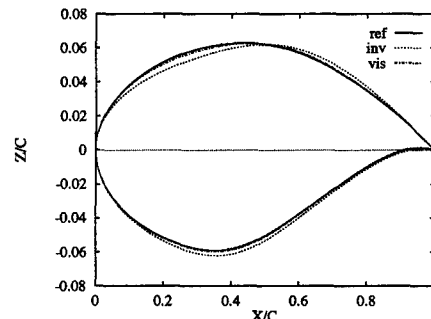


Figure 4: Problem TE3 - Comparison of Initial and Optimised Contours.

Inviscid Optimisation: The computation has been performed using an unstructured grid of 7809 triangles and 4009 nodes. Instead of rebuilding the grid each time the airfoil shape is modified, mesh deformation was provided by the Laplacian smoothing based node movement algorithm. The "best design" was reached after 69 functional evaluations resulting in a reduction of the initial drag coefficient which was driven down from its initial value of 0.00746 to 0.00096. The new shape shows a redesign of the camberline with very high negative value of the camber and a thinner thickness distribution in the first 40 % of the chord, while the thickness increases in the remaining 60 %. The maximum thickness location moves towards the

trailing edge to reach nearly 40 % of the chord (38 % for RAE2822 airfoil). The C_p distribution on the leeward side of the optimised airfoil is characterised by an increase of the suction peak and a reduction of the shock jump; the windward side remains almost unchanged.

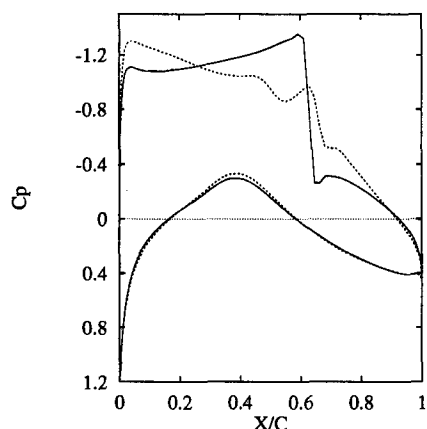


Figure 5: Problem TE3 - Transonic Inviscid Drag Minimisation - Comparison of Pressure Distributions.

Viscous Optimisation: The computation has been performed on an almost structured grid of 8200 elements and 8360 nodes. Here again, mesh deformations were obtained using the node movement algorithm. The "best design" was reached after 68 functional evaluations resulting in a reduction of 7 drag counts ($c_d = 0.0081$ instead of 0.0088). The shape is closer to the RAE2822 airfoil than those coming from inviscid optimisation. Here again, reduction of drag is mainly obtained by the redesign of the camberline but in a lower measure. The thickness distribution remains almost unchanged. The C_p distribution is characterised by a slightly higher suction peak and is shock free.

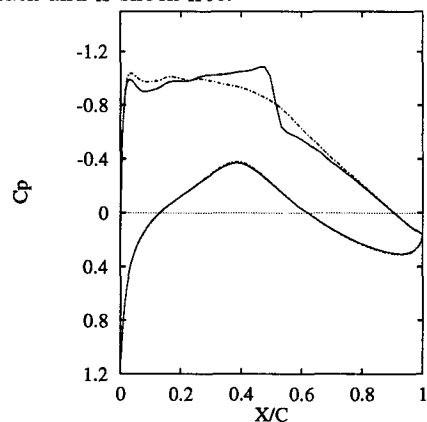


Figure 6: Problem TE3 - Transonic Viscous Drag Minimisation - Comparison of Pressure Distributions.

6.2 Multi-point airfoil optimisation

The problems consist in the improvement of an already existing airfoil in order to increase its maximum speed without deteriorating its characteristics at lower speeds. More precisely, the design problem was defined as to minimize drag at $M_\infty = 0.8$ and $C_l = C_l^*$, maintaining the C_l and C_d characteristics on the buffet onset curve of the original airfoil for $M_\infty = 0.55, 0.62, 0.71, 0.754$, which results in a five-point optimisation problem. The value of

the Mach number is $24 \cdot 10^6$ and the flow is assumed to be fully turbulent.

The new shape is obtained by a redesign of the camberline with higher values of the camber on both leading and rear parts of the airfoil, while the thickness is increased beyond 40% of the chord. The maximum thickness position moves from 35% to 42% of the airfoil chord.

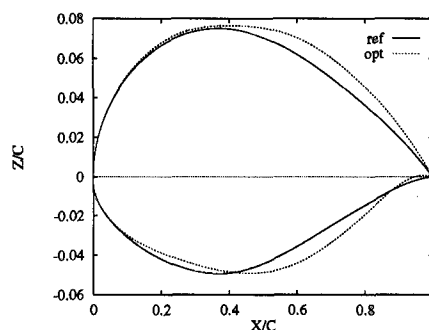


Figure 7: Multi-Point Optimisation - Comparison of Initial and Optimised Contours.

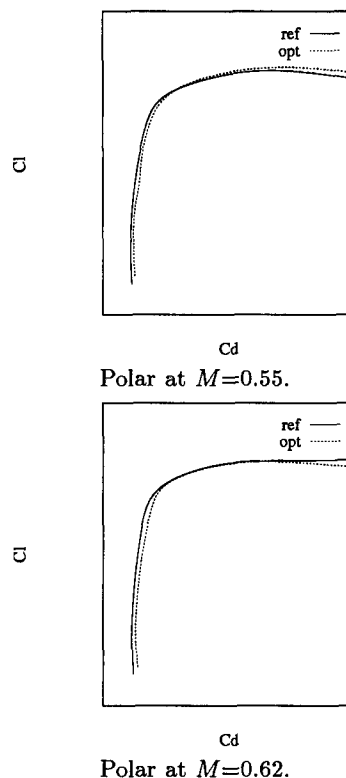


Figure 8: Multi-Point Optimisation - Comparison of Aerodynamic Characteristics.

Figures 8 and 9 illustrate the aerodynamic characteristics ($C_l - C_d$ polars) of the two airfoils. At the main design point ($M = 0.80$), the drag is reduced along the overall lift range. For the secondary points, a small penalty on the drag (a few counts) is observed for low and intermediate values of the lift, while the drag is reduced at higher values. In general, an increase of the maximum lift of the airfoil is reached. This is particularly true at $M = 0.71$ and $M = 0.754$.

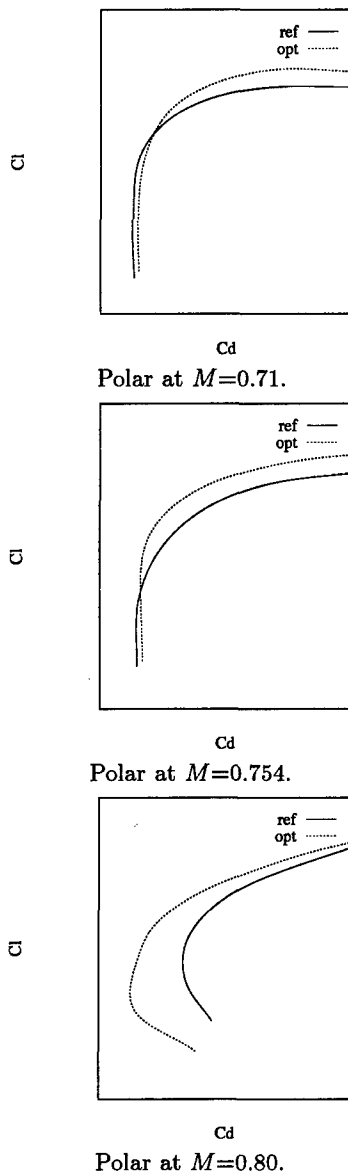


Figure 9: Multi-Point Optimisation - Comparison of Aerodynamic Characteristics.

6.3 Transonic wing optimisation

The reference aircraft geometry selected within the MDO project [6] is representative of a wide-body civil transport aircraft (650 passengers), with a wing span of nearly 80 meters and a maximum take-off weight of about 550 tons. The wing, whose exposed right component planform is illustrated in Fig. 10, has an area of 725 m^2 , an aspect-ratio of 8.2, a span of 77.1 m and a sweep angle of 33° .

The optimisation problem, which has been solved, is summarized as follows:

Design Operation	Economic Cruise ($M_\infty = 0.85$, $C_l^{tot} = 0.458$)
Objective Function	$\Delta DOC = \Delta D + \Delta W$
Constraints	$C_l = C_l^t$ $C_m = C_m^t$
Design Space	Crank and Tip section shapes; Crank thickness

where ΔD is the change of the wing-body drag expressed

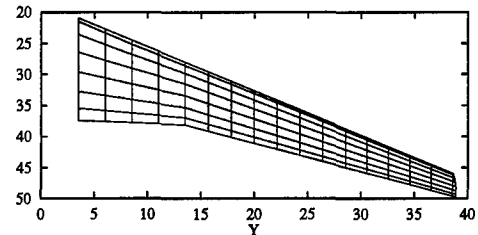


Figure 10: MDO wing - Planform View.

in counts and ΔW is the change in mass of one torsion box expressed in tons.

Starting from a reference trimmed configuration, the problem of reducing the *DOC* by only operating on the wing geometry without modifying other parts of the airplane is thus addressed. The trim condition is satisfied by maintaining the same angle of attack, the same lift and the same pitch moment than those of the original configuration. The root section is kept fixed. Crank and tip wing sections just as the crank thickness are allowed to change, which corresponds to 21 design variables. In addition, it is assumed that crank thickness modification induces the same percentage change in tip thickness.

The structural wing model consists in a centre wing box which is integrally built into the centre fuselage to which are attached the port and starboard lateral wing sections. The centre wing box is a conventional metallic structure with three spars. The structural optimisation model of the wing uses 156 design variables involving size parameters. The finite element model is formed by around 12000 elements. A fine grid of 54 blocks and about 204000 cells has been built around the wing body configuration. It is used to compute the trim condition of the reference geometry and to verify the aerodynamic characteristics of the optimised one. A coarse grid, which is the eighth of the fine, has been implemented into the optimisation system in order to maintain the overall optimisation cost at a reasonable level. For the same reason, the optimised wing mass was approximated by a curve fit as function of the crank thickness.

Table 1: Aerodynamic performance of the optimised configurations.

Case	Config.	C_l	C_m	C_d
Ref	w-b coarse grid	0.4946	-0.1963	0.02120
	w-b fine grid	0.5131	-0.2047	0.01700
	exposed wing	0.4550	-0.1835	0.01390
Opt	w-b coarse grid	0.4928	-0.1957	0.01790
	w-b fine grid	0.5154	-0.2049	0.01370
	exposed wing	0.4579	-0.1848	0.01060

The reduction of drag only results from a reduction of the wing wave drag, as it was expected from the problem definition. Aerodynamic performances of fuselage and tail are maintained unchanged. The use of a coarse grid seems to be adequate since the drag variation between the reference geometry and the optimised one is nearly the same for the two grids.

The improved configuration is obtained after a few global iterations of the optimisation process, which nevertheless corresponds to around 150 functional evaluations. The *DOC* is reduced while meeting the constraints at each iterations.

Table 2: Wing section thickness (%) and wing mass (Kg) of the optimised configurations.

Case	RootTc	CrankTc	TipTc	Wing Mass
Ref	14.00	10.00	8.800	28764
Opt	14.00	8.785	7.730	30562

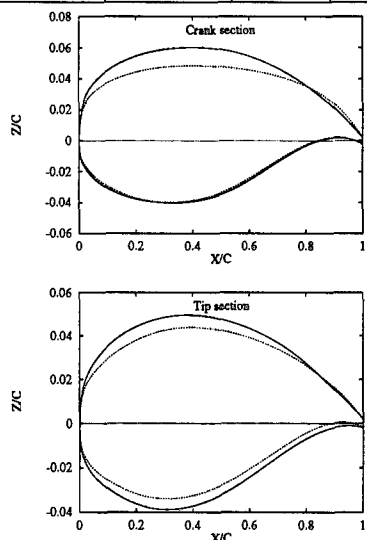


Figure 11: MDO wing - Comparison of Initial and Optimised Contours.

For the optimised geometry, the upper surface of the crank section is flattened. This effect has been mainly obtained by the redesign of the camber line. Except the decrease in the maximum thickness, the thickness distribution is only slightly altered in the rear part of the airfoil. In the case of the tip section, the major changes again apply on the camberline, with a tiny reduction of the leading edge curvature in the thickness distribution. The sectional pressure plots indicate a movement towards a two-shock structure on the upper surface.

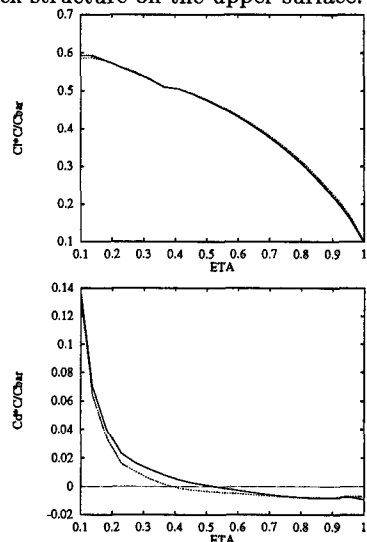


Figure 12: MDO wing - Comparison of Span Loads.

Spanwise loads distributions display a decrease of the drag in the central part of the wing, where lift and pitch moment are approximatively maintained at the same level than those of the reference wing. The loss of lift in the inboard part of the wing is recovered by the outboard sections. The opposite behaviour is found on the pitch moment. By comparison with the problem without

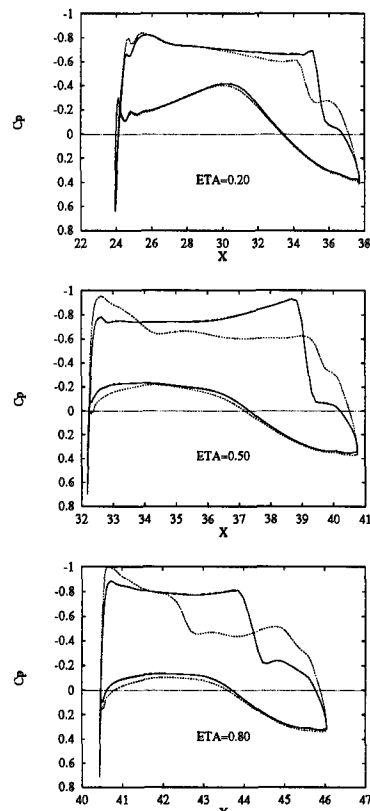


Figure 13: MDO wing - Comparison of Pressure Distributions.

crank thickness modification, the reduction of crank section thickness has the effect of further reducing drag not only in the central part of the wing, but also inboard. It leads nevertheless to an increase of the wing mass.

7 CONCLUSION

Mono- and Multi-disciplinary capability of the optimisation system has successfully been demonstrated for 2D and 3D applications. The capability of the design tool to be able to account for explicit constraints and multi-objectives within the optimisation process is of paramount importance for industrial applications. Nevertheless, the cost of sensitivities is a key factor when advanced modelling methods are used. Cheaper sensitivities and parallel implementations are requested. Future works will involve

1. more accurate gradients computation (adjoint equations, use of automatic differentiation),
2. introduction of other disciplines within the design loop (aeroelasticity, electromagnetism, ...).

8 ACKNOWLEDGEMENTS

Part of this work was performed within MDO project: a collaboration between British Aerospace, Aerospaiale, DASA, Dassault, SAAB, CASA, Alenia, Aerma-cchi, HAI, NLR, DERA, ONERA and the Universities of Delft and Cranfield. The project was funded by the CEC under the BRITE-EURAM initiative (Project Ref: BE95-2056).

References

- [1] Vanderplaats, G.N., *ADS - A Fortran Program for Automated Design Synthesis*, User Manual, 1987.
- [2] Vanderplaats, G.N., *Numerical Optimization Techniques for Engineering Design*, McGraw-Hill Series in Mechanical Engineering.
- [3] Hicks, R. and Henne, P.A., *Wing Design by Numerical Optimization*, Journal of Aircraft, vol 35, n. 7, 1978.
- [4] Farin, G., *Curves and Surfaces for Computer Aided Geometric Design*, Academic Press, 1989.
- [5] Periaux J. et al eds., *Optimum Aerodynamic Design and Parallel Navier-Stokes Computations*, Vieweg, 1998.
- [6] Allwright S., *MDO Process and Specification for the Primary Sensitivity Study*, MDO Technical Report MDO/SPEC/BAE/SA960430, 1996.

DISCUSSION

Session III, Paper #20

Prof Slooff (NLR, Netherlands) noted that in their work, optimising on the basis of Euler equations often led to non-unique solutions, that is several minima of about the same level. In such cases the additional constraints helped to reduce or eliminate this "non-uniqueness". Had the authors encountered this problem?

Dr Selmin indicated no specific experience of this issue, but agreed that adding constraints should help. He saw this as a requirement for a more precise definition of the original design problem.

Mr Perrier (Dassault, France) asked how better predictions of sensitivity could be ensured as he believed that decisions on constraints should come from good knowledge of constraint sensitivity.

Dr Selmin noted that his team intended to improve prediction of sensitivity by moving from the use of finite differences to automatic differentiation to evaluate the gradients.